Domain-Wall Motion Driven by Laplace Pressure in Co-Fe-B/MgO Nanodots with Perpendicular Anisotropy

Yu Zhang,[1,2,3,*] Xueying Zhang,[1,2,3,*] Nicolas Vernier,[3] Zhizhong Zhang,[1,2] Guillaume Agnus,[3] Jean-René Coudevylle,[3] Xiaoyang Lin,[1,2] Yue Zhang,[1,2] You-Guang Zhang,[1,2] Weisheng Zhao,[1,2,†] and Dafiné Ravelosona[3]

[1]*Fert Beijing Research Institute, BDBC, Beihang University, Beijing 100191, China*
[2]*School of Electronic and Information Engineering, Beihang University, Beijing 100191, China*
[3]*Centre de Nanosciences et de Nanotechnologies, University of Paris-Sud, CNRS, Orsay 91405, France*

(Received 29 November 2017; revised manuscript received 20 April 2018; published 18 June 2018)

We study the magnetization reversal of Co-Fe-B/MgO nanodots with perpendicular anisotropy of size ranging from $w = 400$ nm to 1 μm. Contrary to previous experiments, the switching field distribution is shifted toward lower magnetic fields as the size of the elements is reduced with a mean switching field varying as $1/w$. We show that this mechanism can be explained by the nucleation of a pinned magnetic domain wall (DW) at the edges of the nanodots where damages are introduced by the patterning process. As the surface tension (Laplace pressure) applied on the DW increases when reducing the size of the nanodots, we demonstrate that to reverse the entire elements, the depinning field varies as $1/w$. These results suggest that the presence of DWs must be considered in the switching process of nanoscale elements and open a path toward scalable spintronic devices.

DOI: 10.1103/PhysRevApplied.9.064027

I. INTRODUCTION

Magnetic nanostructures based on perpendicular magnetic anisotropy (PMA) [1,2] materials are attracting much attention for their potential applications, such as high-density magnetic random-access memory (MRAM) [3–5], bit-patterned media [6,7], magnetic logic [8–10], and in the fields of magnonics and spin waves [11,12]. The scalability of these applications for ultimate technology nodes is, in general, limited by the structural variability of the nanostructures. This variability leads to a dispersion of the magnetic properties, which strongly affects the switching mechanism when the dimension of the nanostructures becomes smaller. In particular, the mechanism has been extensively shown for the switching process of magnetic dots [13–18]. When the size of the dots is sufficiently large, the dominant mechanism for switching has been found to be nucleation followed by rapid propagation of magnetic domain walls (DWs). In this case, as the propagation fields are usually lower than the nucleation fields [13,19], the switching field distribution (SFD) corresponds to the distribution of the nucleation fields, which is related to the distribution of magnetic anisotropy in the films. As the size of the dot decreases, the SFD is enlarged and shifted toward higher fields. A simple model taking into account the initial intrinsic distribution of magnetic anisotropy in the films can explain these results [14,15]. In addition to such a variability of magnetic properties in the pristine films, edge damages introduced by the patterning process can also have a strong influence on the switching behavior [16]. This situation is the case for spin-transfer-torque MRAM or domain-wall-based nanodevices where the edges have been found to reduce the efficiency of the switching process at small dimensions [20–22].

Here, we use magneto-optic Kerr imaging microscopy [23,24] to study the magnetization reversal of magnetic nanodots based on Co-Fe-B/MgO materials with PMA ranging in size from 400 nm to 1 μm. Contrary to previous results [15,16], we observe that the SFD is shifted toward lower magnetic fields when the size is reduced. Using the framework of elastic interface (e.g., soap bubbles), we show that the Laplace pressure applied on a DW nucleated and pinned at the edges of the nanodots is responsible for such a mechanism.

II. EXPERIMENTAL METHODS AND RESULTS

Co-Fe-B/MgO-based multilayers Ta(5 nm)/CuN(40 nm)/Ta(5 nm)/$Co_{40}Fe_{40}B_{20}$(1.1 nm)/MgO(1 nm)/Ta(5 nm) are grown by sputtering using a Singulus TIMARIS cluster tool on 100-mm Si wafers. After the deposition, the samples are annealed in high vacuum at 380 °C for 20 min. Nanodots of different sizes are patterned by electron-beam lithography using a polymethylmethacrylate (PMMA) resist. Subsequently, a 50-nm-thick Al mask is deposited by electron-beam evaporation onto the film and then lifted off. An ion milling process with Ar ions (etching angle of 45°) is used to pattern the magnetic dots. The magnetic properties of the

*These authors contributed equally to this work.
†To whom all correspondence should be addressed.
weisheng.zhao@buaa.edu.cn

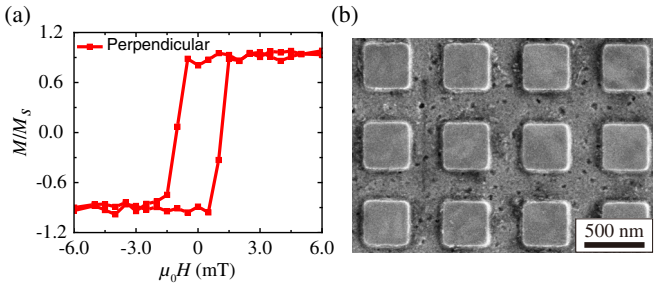

FIG. 1. (a) Hysteresis loops with out-of-plane magnetic field for Ta(5 nm)/CuN(40 nm)/Ta(5 nm)/$Co_{40}Fe_{40}B_{20}$(1.1 nm)/MgO(1 nm)/Ta(5 nm) films. (b) SEM image of a patterned 400-nm nanodot array.

continuous thin films are studied by using a vibrating-sample-magnetometer (VSM) system. The switching process of the nanodots is investigated by using magneto-optic Kerr imaging microscopy with a wavelength of 450 nm [23]. All experiments are performed at room temperature.

Figure 1(a) shows the hysteresis loop of the full films indicating a PMA. The coercivity of the Co-Fe-B layer is as low as $\mu_0 H_c = 1$ mT, as we have shown in our previous study [19]. The effective anisotropy constant of our films is $K_{\text{eff}\,1} = 1.3 \times 10^5$ J/m^3 as calculated by VSM measurement using in-plane magnetic field. Considering the resolution limit of our magneto-optic Kerr microscope, the minimum size of the nanodots fabricated in this work is 400 nm, as shown in Fig. 1(b). The pitch (defined as the distance between the centers of two nanodots) is chosen to be 5 μm to minimize the influence of dipolar effects [25].

In order to characterize the switching process, the following procedure is employed: The film is first saturated with a large positive magnetic field along the perpendicular direction (easy axis), and then a negative magnetic field pulse with a duration of 1 ms is applied to investigate the switching process by Kerr microscopy. The above procedure is repeated and for different negative magnetic field pulse, the number of reversed islands is counted. The switching probability of the array is then obtained by calculating the ratio of the reversed nanodots to the overall number of nanodots. Figure 2 shows the typical magnetic switching process of the nanodot arrays for sizes of 1 μm and 600 nm, respectively. As expected, due to the variability of the nanoelements, a SFD is observed. For instance, for the 1 μm nanodots [see Fig. 2(a)], nearly 10% and 90% of the nanodots are reversed under magnetic fields of 11 and 16 mT, respectively. Surprisingly, we observe that for the array of 600-nm nanodots, the SFD is shifted to lower magnetic fields. In this latter case, nearly 10% and 90% of the nanodots are reversed under magnetic fields of 9 and 12 mT, respectively. The SFD measurements are repeated several times for each dimension and are reproducible within a variation of 2%.

The number of switched islands for the 1-μm and 600-nm nanodots is presented in Figs. 3(a) and 3(b), respectively. In addition to the shift of the SFD to lower magnetic fields for

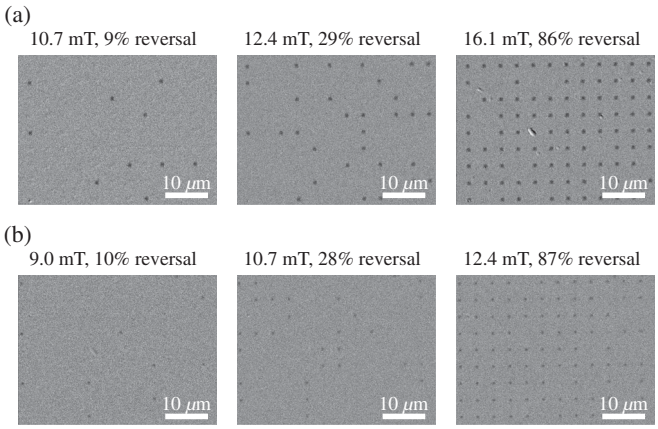

FIG. 2. Kerr microscopy images showing the switching process under magnetic fields for the nanodot arrays of sizes (a) 1 μm and (b) 600 nm.

the smaller nanodots, we observe that the shape of the distribution is roughly unmodified. In order to fit the data, we use the method based on integrated Gaussian distribution fits [16], where the cumulative distribution function with an error function $\text{erf}(x) = [2/(\sqrt{\pi})] \int_0^x e^{-t^2} dt$ is defined as

$$P(H) = \frac{1}{2}\left[1 + \text{erf}\left(\frac{H - H_{\text{SF}}}{\sigma\sqrt{2}}\right)\right]. \quad (1)$$

Then, the average switching field (mean) H_{SF} and the width of the distribution (standard deviation) σ can be determined precisely, as shown in Fig. 3(c) and Table I.

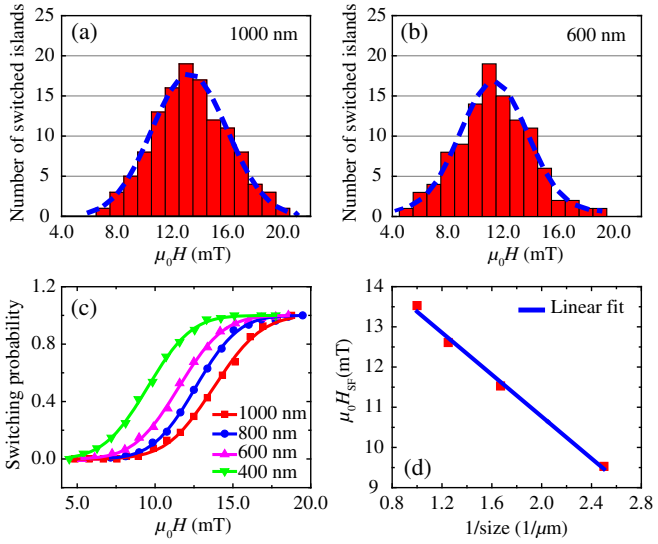

FIG. 3. Histogram indicating the number of islands that switch as a function of the applied magnetic field for a dot size of (a) 1 μm and (b) 600 nm. (c) Average switching probability as a function of magnetic field for dot sizes of 1 μm, and 800, 600, and 400 nm. (d) Average switching field as a function of the inverse of the dot size.

TABLE I. Average switching field and width of the distribution as a function of the dot size.

Dot size (nm)	1/size (μm^{-1})	Average switching field[a] (mT)	Width of the distribution[a] (mT)
400	2.50	9.5	2.2
600	1.67	11.5	2.3
800	1.25	12.6	2.2
1000	1.00	13.5	2.4

[a]Average switching field H_{SF} and the width of the distribution σ are obtained by extracting the parameters from experimental data (see Fig. 3).

Consistent with Fig. 2, we observe a clear shift of the SFD toward lower fields when the size is reduced without noticeable change of the width of the distribution σ approximately 2 mT. In addition, Fig. 3(d) indicates a linear relationship between the average switching field H_{SF} and the inverse of the dot size w.

In order to understand why the SFD shifts to lower magnetic fields when reducing the size of the nanodots, the multilayers with identical stacks are patterned into 400-μm-large squares under the same fabrication process. As shown in Fig. 4(a), after a magnetic field pulse of a few microseconds, although a few nucleation sites are present inside the squares as expected for much larger structures, we observe that most of the nucleation and propagation events occur along the edges. This result suggests the existence of a region of lower anisotropy at the edges of the elements that channels both DW nucleation and motion [26–28]. We believe that this feature is due to the patterning process [16,24,29–33], in particular, the Ar ion milling that induces damages such as edge roughness, redeposition on the sidewall, intermixing of the interfaces, or oxidation of the layers. In addition, owing to the difference in etching rate, the material segregation of Co-Fe-B may lead to the different compositions of Co and Fe at the edges as well [19,23]. The damaged region is, in general, of the order of the grain size, which corresponds to a typical length scale of 10–20 nm [34,35].

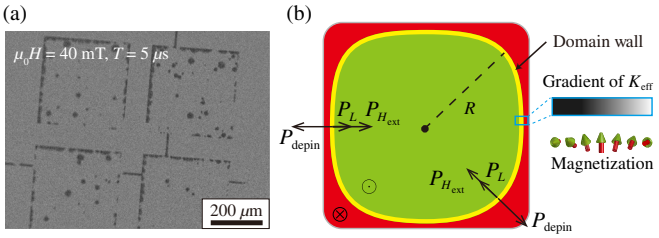

FIG. 4. (a) Kerr microscopy image of large squares (size of 400 μm) indicating the presence of nucleation events. The sample is first saturated with a strong magnetic field, and then an opposite field of 40 mT is applied for 5 μs. (b) Schematic of the magnetization reversal process of a nanodot as described in the text. A single domain wall (yellow) is located at the edge of the dot, separating the reversed (red) and nonreversed regions (green). The DW is pinned by a gradient of anisotropy on a length scale of $\delta \sim \Delta$ due to edge damages. P_{depin}, $P_{H_{ext}}$, and P_L correspond to the pressures applied on the DW due to the pinning, the external magnetic field, and the Laplace pressure, respectively.

III. DISCUSSION

Below, we show that our results can be explained by the pinning of the DW at the edges of the nanodots together with the action of a Laplace pressure on the DW. First, as demonstrated previously [36], the presence of a gradient of anisotropy with a scale of the DW width Δ can induce strong DW pinning. In particular, if we consider a DW pinned at the edges of the nanodots, the depinning field is given by

$$\mu_0 H_{depin} = \frac{K_{eff\,1} - K_{eff\,2}}{2M_s} \frac{2\Delta}{\delta} \tanh\left(\frac{\delta}{2\Delta}\right), \qquad (2)$$

where $K_{eff\,1}$ and $K_{eff\,2}$ are the effective anisotropy in the nondamaged and damaged areas respectively, δ is the gradient length, M_s is the volume saturation magnetization, and Δ is the DW width. In particular, for δ with the same order of Δ, a variation of a few 10% of the anisotropy can give depinning fields of the order of a few 10 mT, which is much larger than the ultralow intrinsic depinning fields of the films (approximately 2 mT) [19]. As a result, once reversed domains are nucleated at the edges, they are expected to propagate only along the edges as shown in Fig. 4(a), and not toward the center of the nanodots (i.e., they cannot go across the pinning potential).

As we have evidenced recently, the Laplace pressure plays an important role in the dynamic of curved DWs [37]. This pressure originates from the DW surface tension [38–40], which is a mechanism quite well known for soap bubbles [41,42]. Once the curvature radius of a DW becomes smaller than several micrometers, this pressure can be high enough to dominate the dynamic of DWs, such as inducing the spontaneous collapse of a domain bubble. In the following, we further describe the depinning process to reverse the entire nanodot by introducing Laplace pressure on the DW. Because of the lower anisotropy induced by the etching process, the DWs first nucleate at the edges of the dots. Note that the duration of the applied magnetic field pulse is 1 ms, which is sufficiently long for the nucleated DWs to propagate along the edges, even with a low speed in the creep regime. Then, the nucleated DWs are connected with each other and form a single DW along the edge of the dot. Note that in magnetic reversal, in addition to the driving magnetic field, a Laplace pressure is applied on the DWs with curvature (i.e., an arc-shaped DW at the edge of the dots). This pressure favors the collapse of the DW into the center of the dot, and its strength is inversely proportional to the radius of curvature R of the

DW. Considering a circular DW of radius $R = w/2$ at the edges of the nanodot, the Laplace pressure expresses as

$$P_L = 2\lambda/w, \tag{3}$$

where λ is the interfacial energy density of the pinned DW. We note that for Bloch-type domain walls, the interfacial energy density can be written as $\lambda = 4(A_s K_{\text{eff}\,2})^{1/2}$, where A_s is the exchange stiffness constant. When an external magnetic field H_{ext} is applied along the perpendicular direction, the Zeeman energy induces a pressure on the DW that can be written as

$$P_{H_{\text{ext}}} = 2M_s\mu_0 H_{\text{ext}}. \tag{4}$$

The Zeeman energy and the Laplace pressure act together to depin the domain wall as illustrated in Fig. 4(b), which gives

$$P_L + P_{H_{\text{ext}}} = 2M_s\mu_0 H_{\text{depin}}. \tag{5}$$

By combining Eqs. (3)–(5), this gives the minimum switching field H_{SF} to overcome the pinning potential as

$$\mu_0 H_{\text{SF}} = \mu_0 H_{\text{depin}} - \frac{\lambda}{M_s}\frac{1}{w}. \tag{6}$$

This result is in agreement with the linear variation experimentally observed in Fig. 3(d) and indicates that the Laplace pressure just acts as a simple effective field proportional to $1/w$, which shifts only the distribution without modifying its width σ. Using a linear fit allows us to determine $\mu_0 H_{\text{depin}}$ and λ/M_s. We find $\mu_0 H_{\text{depin}} =$ 16 mT and a DW energy $\lambda = 3.4 \times 10^{-3}$ J/m^2, which is in very good agreement with previous studies [37,43]. Finally, by considering $\mu_0 H_{\text{depin}} = 16$ mT, a typical gradient of $\delta \sim \Delta$, the experimental values $K_{\text{eff}\,1} = 1.3 \times 10^5$ J/m^3 and $M_s = 1.3 \times 10^6$ A/m, Eq. (2) gives $K_{\text{eff}\,2} = 8.5 \times 10^4$ J/m^3. These results indicate that due to patterning-induced damages, a gradient of anisotropy of about 30% is present at the edges of the nanodots on a length scale of the DW width.

IV. CONCLUSION

In conclusion, we demonstrate that due to the presence of edge damages, the DW nucleation and depinning process govern the field-induced magnetic reversal of nanodots. The Laplace pressure plays a critical role in explaining the decreased SFD with the reduced size of the dots. Those features should be taken into account in advanced spintronic devices such as spin-orbit-torque MRAM where the spin current can also induce the nucleation of DWs at the edges of the elements. These results suggest a path toward scalable devices based on controlling the nucleation and pinning potential of DWs at the edges of the nanoelements. In this case, benefiting from the Laplace pressure and keeping the same thermal stability given by the gradient of anisotropy, a lower switching current is needed when reducing the size of the devices.

ACKNOWLEDGMENTS

The authors thank Daoqian Zhu and Jiaqi Wei for technical support as well as constructive discussion. We gratefully acknowledge financial support from the European Union FP7 program (ITN WALL Grant No. 608031), the French National Research Agency (COMAG, ELECSPIN), as well as International Collaboration Projects (Grants No. 2015DFE12880 and No. B16001) and Special Foundation of Beijing Municipal Science & Technology Commission (Grant No. Z161100000216149).

[1] F. Hellman *et al.*, Interface-induced phenomena in magnetism, Rev. Mod. Phys. **89**, 025006 (2017).
[2] A. G. Kolesnikov, A. S. Samardak, M. E. Stebliy, A. V. Ognev, L. A. Chebotkevich, A. V. Sadovnikov, S. A. Nikitov, Y. J. Kim, I. H. Cha, and Y. K. Kim, Spontaneous nucleation and topological stabilization of Skyrmions in magnetic nanodisks with the interfacial Dzyaloshinskii-Moriya interaction, J. Magn. Magn. Mater. **429**, 221 (2017).
[3] S. Ikeda, K. Miura, H. Yamamoto, K. Mizunuma, H. D. Gan, M. Endo, S. Kanai, J. Hayakawa, F. Matsukura, and H. Ohno, A perpendicular-anisotropy CoFeB-MgO magnetic tunnel junction, Nat. Mater. **9**, 721 (2010).
[4] A. D. Kent and D. C. Worledge, A new spin on magnetic memories, Nat. Nanotechnol. **10**, 187 (2015).
[5] Y. Zhang, W. Cai, W. Kang, J. Yang, E. Deng, Y.-G. Zhang, W. Zhao, and D. Ravelosona, Demonstration of multi-state memory device combining resistive and magnetic switching behaviors, IEEE Electron Device Lett. **39**, 684 (2018).
[6] D. O'Connor and A. V. Zayats, Data storage: The third plasmonic revolution, Nat. Nanotechnol. **5**, 482 (2010).
[7] T. R. Albrecht *et al.*, Bit-patterned magnetic recording: Theory, media fabrication, and recording performance, IEEE Trans. Magn. **51**, 1 (2015).
[8] J. Torrejon, M. Riou, F. A. Araujo, S. Tsunegi, G. Khalsa, D. Querlioz, P. Bortolotti, V. Cros, K. Yakushiji, A. Fukushima, H. Kubota, S. Yuasa, M. D. Stiles, and J. Grollier, Neuromorphic computing with nanoscale spintronic oscillators, Nature (London) **547**, 428 (2017).
[9] A. V. Sadovnikov, A. A. Grachev, E. N. Beginin, S. E. Sheshukova, Y. P. Sharaevskii, and S. A. Nikitov, Voltage-Controlled Spin-Wave Coupling in Adjacent Ferromagnetic-Ferroelectric Heterostructures, Phys. Rev. Applied **7**, 014013 (2017).
[10] A. V. Sadovnikov, S. A. Odintsov, E. N. Beginin, S. E. Sheshukova, Y. P. Sharaevskii, and S. A. Nikitov, Toward nonlinear magnonics: Intensity-dependent spin-wave switching in insulating side-coupled magnetic stripes, Phys. Rev. B **96**, 144428 (2017).

[11] C. S. Davies, A. V. Sadovnikov, S. V. Grishin, Yu. P. Sharaevskii, S. A. Nikitov, and V. V. Kruglyak, Generation of propagating spin waves from regions of increased dynamic demagnetising field near magnetic antidots, Appl. Phys. Lett. **107**, 162401 (2015).

[12] C. S. Davies, A. V. Sadovnikov, S. V. Grishin, Yu. P. Sharaevsky, S. A. Nikitov, and V. V. Kruglyak, Field-controlled phase-rectified magnonic multiplexer, IEEE Trans. Magn. **51**, 1 (2015).

[13] G. Hu, T. Thomson, C. T. Rettner, and B. D. Terris, Rotation and wall propagation in multidomain Co/Pd islands, IEEE Magn. Lett. **41**, 3589 (2005).

[14] G. Hu, T. Thomson, C. T. Rettner, S. Raoux, and B. D. Terris, Magnetization reversal in Co/Pd nanostructures and films, J. Appl. Phys. **97**, 10J702 (2005).

[15] T. Thomson, G. Hu, and B. D. Terris, Intrinsic Distribution of Magnetic Anisotropy in Thin Films Probed by Patterned Nanostructures, Phys. Rev. Lett. **96**, 257204 (2006).

[16] J. M. Shaw, S. E. Russek, T. Thomson, M. J. Donahue, B. D. Terris, O. Hellwig, E. Dobisz, and M. L. Schneider, Reversal mechanisms in perpendicularly magnetized nanostructures, Phys. Rev. B **78**, 024414 (2008).

[17] S. Okamoto, N. Kikuchi, M. Furuta, O. Kitakami, and T. Shimatsu, Switching Behaviors and Its Dynamics of a Co/Pt Nanodot under the Assistance of rf Fields, Phys. Rev. Lett. **109**, 237209 (2012).

[18] H. Suto, T. Nagasawa, K. Kudo, T. Kanao, K. Mizushima, and R. Sato, Layer-Selective Switching of a Double-Layer Perpendicular Magnetic Nanodot Using Microwave Assistance, Phys. Rev. Applied **5**, 014003 (2016).

[19] C. Burrowes, N. Vernier, J. P. Adam, L. Herrera Diez, K. Garcia, I. Barisic, G. Agnus, S. Eimer, J. V. Kim, T. Devolder, A. Lamperti, R. Mantovan, B. Ockert, E. E. Fullerton, and D. Ravelosona, Low depinning fields in Ta-CoFeB-MgO ultrathin films with perpendicular magnetic anisotropy, Appl. Phys. Lett. **103**, 182401 (2013).

[20] F. Cayssol, D. Ravelosona, C. Chappert, J. Ferre, and J. P. Jamet, Domain Wall Creep in Magnetic Wires, Phys. Rev. Lett. **92**, 107202 (2004).

[21] K. Kinoshita, H. Honjo, S. Fukami, H. Sato, K. Mizunuma, K. Tokutome, M. Murahata, S. Ikeda, S. Miura, N. Kasai, and H. Ohno, Process-induced damage and its recovery for a CoFeB-MgO magnetic tunnel junction with perpendicular magnetic easy axis, Jpn. J. Appl. Phys. **53**, 103001 (2014).

[22] J. J. Nowak, R. P. Ray, J. Z. Sun, G. Hu, J. H. Park, J. Lee, A. J. Annunziata, G. P. Lauer, R. Kothandaraman, E. J. O. Sullivan, P. L. Trouilloud, Y. Kim, and D. C. Worledge, Dependence of voltage and size on write error rates in spin-transfer torque magnetic random-access memory, IEEE Magn. Lett. **7**, 1 (2016).

[23] N. Vernier, J. P. Adam, S. Eimer, G. Agnus, T. Devolder, T. Hauet, B. Ocker, F. Garcia, and D. Ravelosona, Measurement of magnetization using domain compressibility in CoFeB films with perpendicular anisotropy, Appl. Phys. Lett. **104**, 122404 (2014).

[24] C. J. Durrant, R. J. Hicken, Q. Hao, and G. Xiao, Scanning Kerr microscopy study of current-induced switching in Ta/CoFeB/MgO films with perpendicular magnetic anisotropy, Phys. Rev. B **93**, 014414 (2016).

[25] B. Pfau, C. M. Günther, E. Guehrs, T. Hauet, T. Hennen, S. Eisebitt, and O. Hellwig, Influence of stray fields on the switching-field distribution for bit-patterned media based on pre-patterned substrates, Appl. Phys. Lett. **105**, 132407 (2014).

[26] J.-P. Adam, S. Rohart, J.-P. Jamet, A. Mougin, J. Ferré, H. Bernas, G. Faini, and J. Fassbender, Single Pt/Co(0.5 nm)/Pt nano-discs: Beyond the coherent spin reversal model and thermal stability, J. Magn. Soc. Jpn. **33**, 498 (2009).

[27] J.-P. Adam, J.-P. Jamet, J. Ferré, A. Mougin, S. Rohart, R. Weil, E. Bourhis, and J. Gierak, Magnetization reversal in Pt/Co(0.5 nm)/Pt nano-platelets patterned by focused ion beam lithography, Nanotechnology **21**, 445302 (2010).

[28] J.-P. Adam, S. Rohart, J.-P. Jamet, J. Ferré, A. Mougin, R. Weil, H. Bernas, and G. Faini, Magnetization reversal by confined droplet growth in soft/hard hybrid nanodisks with perpendicular anisotropy, Phys. Rev. B **85**, 214417 (2012).

[29] M. T. Johnson, P. J. H. Bloemen, F. J. A den Broeder, and J. J. de Vries, Magnetic anisotropy in metallic multilayers, Rep. Prog. Phys. **59**, 1409 (1996).

[30] H. X. Yang, M. Chshiev, B. Dieny, J. H. Lee, A. Manchon, and K. H. Shin, First-principles investigation of the very large perpendicular magnetic anisotropy at FeMgO and Co|MgO interfaces, Phys. Rev. B **84**, 054401 (2011).

[31] J. W. Lau, R. D. McMichael, M. A. Schofield, and Y. Zhu, Correlation of edge roughness to nucleation field and nucleation field distribution in patterned permalloy elements, J. Appl. Phys. **102**, 023916 (2007).

[32] K. Kinoshita, H. Utsumi, K. Suemitsu, H. Hada, and T. Sugibayashi, Etching magnetic tunnel junction with metal etchers, Jpn. J. Appl. Phys. **49**, 08JB02 (2010).

[33] A. Neumann, A. Frauen, J. Vollmers, A. Meyer, and H. P. Oepen, Structure-induced spin reorientation in magnetic nanostructures, Phys. Rev. B **94**, 094430 (2016).

[34] S. W. Chun, D. Kim, J. Kwon, B. Kim, S. Choi, and S. B. Lee, Multi-step ion beam etching of sub-30 nm magnetic tunnel junctions for reducing leakage and MgO barrier damage, J. Appl. Phys. **111**, 07C722 (2012).

[35] Y. Zhang, X. Lin, J. P. Adam, G. Agnus, W. Kang, W. Cai, J. R. Coudevylle, N. Isac, J. Yang, H. Yang, K. Cao, H. Cui, D. Zhang, Y. G. Zhang, C. Zhao, W. Zhao, and D. Ravelosona, Heterogeneous memristive devices enabled by magnetic tunnel junction nanopillars surrounded by resistive silicon switches, Adv. Electron. Mater. **4**, 1700461 (2018).

[36] J. H. Franken, M. Hoeijmakers, R. Lavrijsen, J. T. Kohlhepp, H. J. M. Swagten, B. Koopmans, E. Van Veldhoven, and D. J. Maas, Precise control of domain wall injection and pinning using helium and gallium focused ion beams, J. Appl. Phys. **109**, 07D504 (2011).

[37] X. Zhang, N. Vernier, W. Zhao, H. Yu, L. Vila, Y. Zhang, and D. Ravelosona, Direct Observation of Domain-Wall Surface Tension by Deflating or Inflating a Magnetic Bubble, Phys. Rev. Applied **9**, 024032 (2018).

[38] P. Gaunt, The frequency constant for thermal activitation of a ferromagnetic domain wall, J. Appl. Phys. **48**, 3470 (1977).

[39] P. Gaunt, Ferromagnetic domain wall pinning by a random array of inhomogeneities, Philos. Mag. B **48**, 261 (1983).

[40] W. Jiang, P. Upadhyaya, W. Zhang, G. Yu, M. B. Jungfleisch, F. Y. Fradin, J. E. Pearson, Y. Tserkovnyak, K. L. Wang, O. Heinonen, S. G. te Velthuis, and A. Hoffmann, Blowing magnetic Skyrmion bubbles, Science **349**, 283 (2015).

[41] C. Isenberg, *The Science of Soap Films and Soap Bubbles*, 2nd ed. (Dover Publications, Inc., New York, 1992).

[42] P.-G. de Genes, F. Brochard-Wyart, and D. Quéré, *Capillarity and Wetting Phenomena* (Springer-Verlag, Inc., New York, 2004).

[43] M. Yamanouchi, A. Jander, P. Dhagat, S. Ikeda, F. Matsukura, and H. Ohno, Domain structure in CoFeB thin films with perpendicular magnetic anisotropy, IEEE Trans. Magn. Lett. **2**, 1 (2011).